Advances in Sciences and Arts
Journal homepage: https://asa.must.ac.mw/

RESEARCH ARTICLE
Vol. 2 Issue 1

Category
Science

Correspondence to:
echinkaka@must.ac.mw

Citation
Chinkaka *et al.* (2025). Mapping Hydrothermal Mineral groups and Geological Structures in the Kirk range - Lisungwe Valley Area in Malawi using ASTER imagery data. Advances in Sciences and Arts. https://doi.org/10.37872/2025.0201.11

Supporting info
Please refer to the journal's official website on https://asa.must.ac.mw/

Received
1st Oct 2024

Accepted
1st Feb, 2025

Published
14th Mar, 2025

DOI
https://doi.org/10.37872/2025.0201.11

Mapping Hydrothermal Mineral groups and Geological Structures in the Kirk range - Lisungwe Valley Area in Malawi using ASTER imagery data

Emmanuel Chinkaka[1,2*], Francis Kapakasa[1], Chikondi Chisenga[1], Richard L.S Mvula[1], Wilson Tchongwe[1] and Kyle F. Davis[2,3]

[1] Department of Earth Sciences, Malawi University of Science and Technology, P.O. Box 5196, Limbe, Malawi
[2]Department of Geography and Spatial Sciences, University of Delaware, Newark, DE 19716, USA
[3]Department of Plant and Soil Sciences, University of Delaware, Newark, DE 19716, USA

Abstract Remote sensing studies have recently been used to aid early stages of mineral exploration and lineament mapping. A multispectral remote sensing sensor known as Advanced Spaceborne Thermal Emission and Reflection Radiometer (ASTER) was used in this research as a main remote sensing data source. ASTER sensor measures reflected radiation in VNIR, SWIR and TIR of the electromagnetic spectrum, which allow identification of various alteration mineral groups. In this paper, 9 bands of ASTER (VNIR-SWIR) data were used to detect alteration mineral groups and geological structures. ASTER band ratio operations were applied to delineate hydrothermal alteration mineral groups and LINE Module algorithm was used to detect geological lineaments on principal component enhanced images. The findings indicate that the band ratio method successfully mapped various alteration mineral zones including FeO minerals (hematite, goethite), Al-OH clay minerals (muscovite, illite, montmorillonite, kaolinite, dickite) and Mg-OH mineral (calcite, dolomite, magnesite, chlorite, epidote, serpentine). The automated lineament extraction method was found suitable for extraction of lineaments from ASTER data as it delineated geological lineaments that are comparable to the existing published lineaments and help in updating the old structural map of the study area. The study suggests that hydrothermal mineralization in the study area is structurally controlled and that further mineral exploration in the Kirk range – Lisungwe area should target the NE-SW geological structures since they represent areas of fluid flow conduits and hydrothermal mineral concentration. This research has presented the potential zones

of mineralization within the Kirk-range Lisungwe Valley area and demonstrated that spectral remote sensing techniques have excellent potential for mineral alteration and structural mapping.

Keywords: *Remote Sensing, Mineral Exploration, Mineralization, Band Ratio, Principal Component Analysis, Hydrothermal Minerals, Kirk range – Lisungwe, Geological lineaments.*

1. Background

Remote sensing has proven valuable in the early stages of mineral exploration studies in alteration mineral mapping. Various deposits of metals are characterized by alteration and mineralization zones (Zhang et al., 2016). This is possible using spectral identification of potential areas of hydrothermal alteration minerals. Hydrothermal alteration minerals with diagnostic spectral absorption properties in the visible and near-infrared through the shortwave infrared regions can be identified by multispectral and hyperspectral remote sensing data. Due to its multispectral scale, the Advanced Spaceborne Thermal Emission and Reflection Radiometer (ASTER) is commonly used to map hydrothermal alteration mineral groups such as clays, phyllosilicates, Sulfates, carbonates, iron oxides, and hydroxides (Gupta, 2003; Testa et al., 2018). ASTER is a sensor on-board the EOS/Terra platform launched by NASA in 1999. It comprises three separate instrument subsystems that operate in different spectral regions. Band 1-3 (VNIR), 4-9 (SWIR), and 10-14 (TIR). The spatial resolution varies depending on the subsystems; VNIR has a resolution of 15m, SWIR 30m, and TIR 90m. Due to the more significant number of bands within the SWIR, this sensor is the first multispectral to discriminate OH-bearing minerals (Mars & Rowan, 2011; Testa et al., 2018).

Alteration mineral and geological structures mapping aid in mineral exploration studies and other geologic studies such as mining. Yong-gui et al., (2014) used ASTER imagery successfully in mapping mineral groups to detect potential mineralized areas using band ratio in Kaladawan area, China. Li et al., (2011) also used ASTER imagery to highlight and map lineament structural information by using principal component analysis compared to other enhancement techniques. Ore deposits are produced mainly by fluid flow processes that normally alter the geochemistry of the country rock. Several previous studies have proved the reliability of multispectral data analysis in the field of alteration mineral mapping and identification. Mapping of alteration mineral groups and the geologic structures has been done in different areas around the world using remote sensing data. Spectral analysis to map hydrothermal alteration groups was done on ASTER data on the Muteh mining area, Iran to map potential mineralization zones (Haroni & Lavafan, 2007). ASTER data has been used in the exploration of mineral deposits by detecting geologic lineaments using various methods (Sukumar & Nelson, 2017).

The Geological events that led to the topography of the Kirk Range - Lisungwe area, for example, rift faulting, various intrusions, metasomatism and hydrothermal activity from Precambrian to Cretaceous, created favourable conditions for mineralization to occur. This area is known to have multiple mineral/metal occurrences of Copper, Gold, Iron Ore, Limestone, Kaolin, and Graphite. To the knowledge of this research, there are no reported remote sensing studies of alteration mapping in the area, and no studies that relate hydrothermal alteration minerals in the area to the geological structures. The overall objective of this study is to map hydrothermal alteration minerals groups in the Kirk-range area, which shall be used in mineral exploration efforts in the area. This work further investigates if the mineral alterations in the study area are structurally controlled. The results are essential for further comprehensive mineral exploration targets in the study area.

1.1. **Location of Study Area**

The study area lies within the southern part of Malawi along the Malawi western border (Figure 1). The Lisungwe – Kirk range valley area is bounded by the 15°00'S and 15°30'S parallels of latitude, the 35 °00'E parallel of longitude and the western border of Malawi with Mozambique (Bloomfield & Garson, 1965).

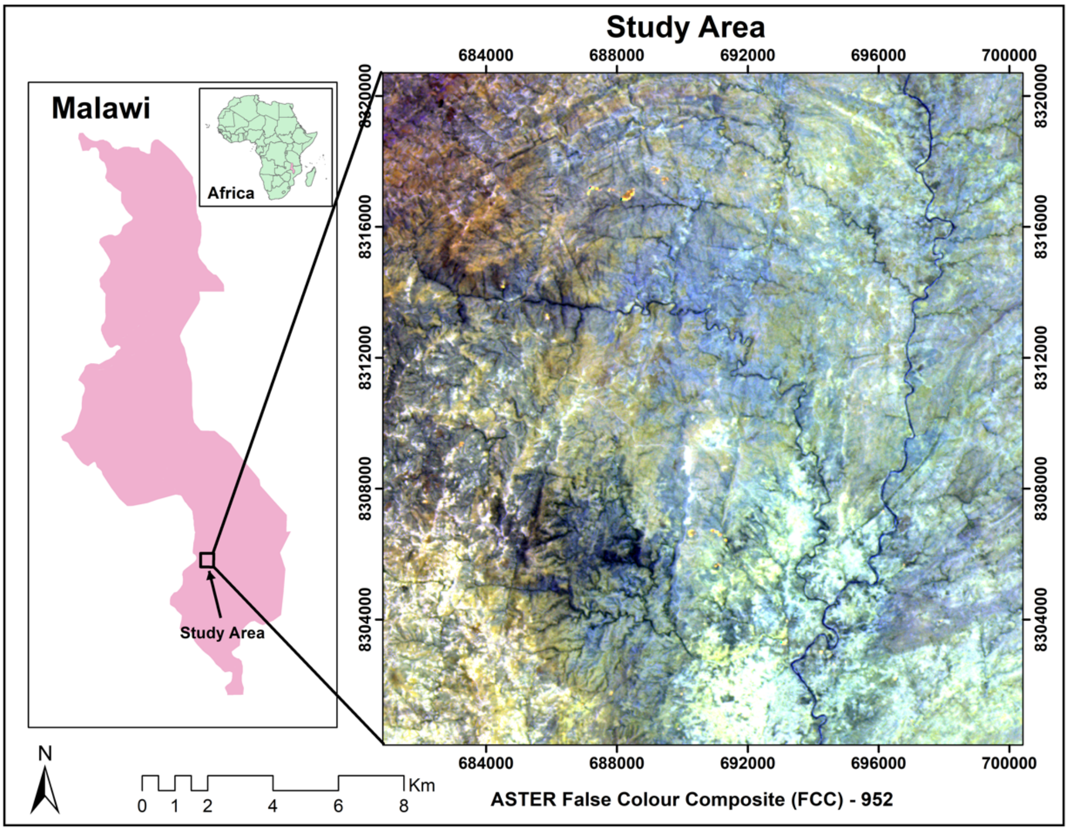

Figure 1: ASTER satellite imagery showing the Kirk Range - Lisungwe Valley in FCC - 952

1.2 Regional geology

The Malawi crust is underlain by rock units that belong to the Precambrian to lower Paleozoic geologic periods (Chisambi & von der Heyden, 2019). These rock units are made up of high-grade metamorphic para- and orthogneisses and schists commonly referred to as Malawi basement complex rocks. The Kirk range – Lisungwe area straddles tectonostratigraphic terranes of Tete-Chipata and Unango Complexes that were formed during the older orogenic episodes of Ubendian and Irumide orogenies (Ring & Betzler, 1993). McConnell (1950) observed that the Ubendian Orogenic mobile belt is characterized by NWW-SEE striking structures and was formed during the Palaeoproterozoic Ubendian Orogeny between 2,200 and 1,800 Ma. While the Mesoproterozoic Irumide Orogeny trends in the northeast direction (Ring & Betzler, 1993).

The area was then affected by the Pan African Orogeny which occurred roughly at 800–500 Ma and is the recent orogeny forming the Mozambiquian Belt (Chisambi & von der Heyden, 2019). This recent orogeny shaped the general geology of Malawi and overprinted older orogenic features from the two previous orogenies (Chiwona et al., 2020). Figure 2 shows the major lithotectonic units in Malawi.

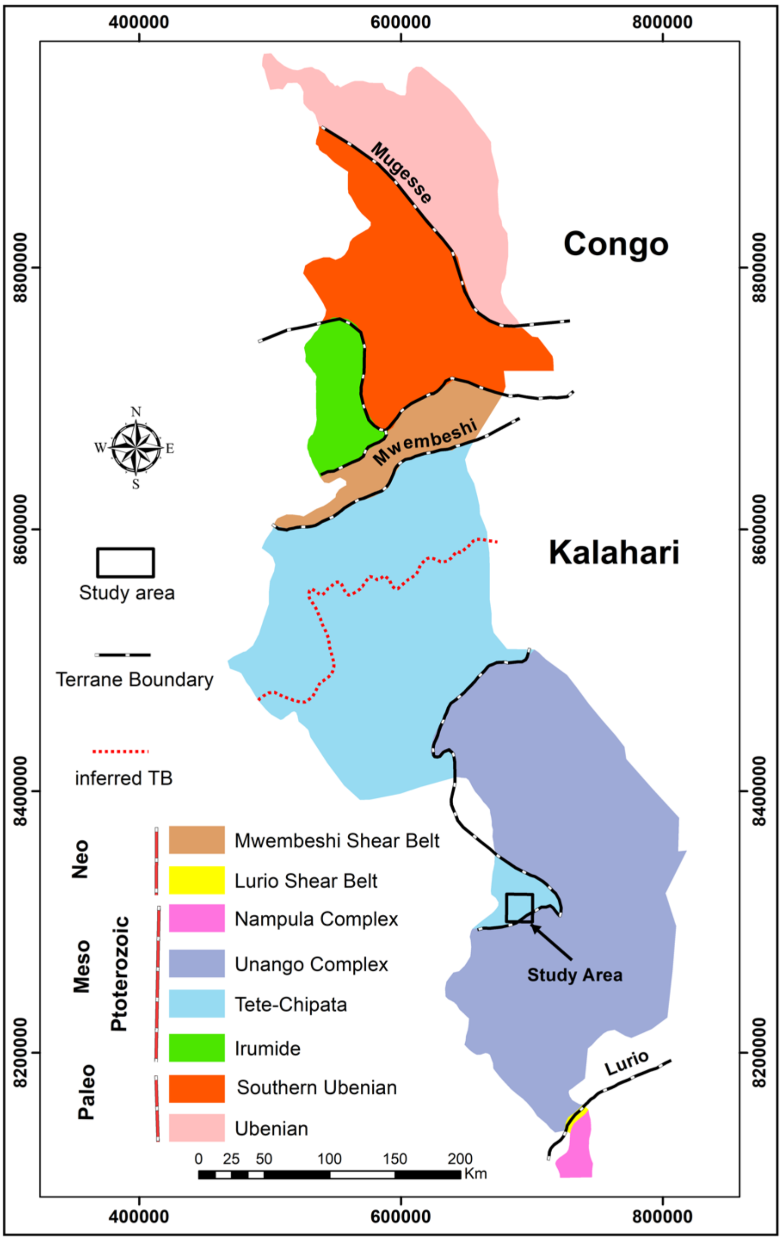

Figure 2: Regional Geology showing the Precambrian Structural architecture

1.3 Local geology

A large part of the area is covered by high-grade paragneisses and schists of the basement complex. These comprise hornblende-biotite-gneisses, often garnetiferous and locally containing a high proportion of various compositions (epidote; biotite gneisses; diopside bearing gneisses; psammitic and pelitic gneisses; charnockitic gneisses; marbles and calc-silicate granulites). A pelitic Kirk Schist Group consists of muscovite-schist members containing kyanite and garnet and often richly graphitic separated by hornblende-biotite gneisses. There is also an unusual calc-pelitic schist formation (Bloomfield & Garson, 1965).

Pre-kinematic intrusions include an extensive series of thin bands of metadolerite and sharply defined belts of anorthositic gneisses. Most of the gneisses may be assigned to the almandine-amphibolite metamorphic facies apart from the small areas of higher grade charnockitic granulite (Bloomfield & Garson, 1965).The paragneisses have been affected by migmatization in many places, and *lit-par-lit* gneisses, secretion pegmatites and boudinage are common. Narrow cross-cutting dykes of pegmatite and aplite are abundant. Schorl-bearing quartz reefs are found, particularly in the north-east of the area (Bloomfield & Garson, 1965).

Syn-kinematic intrusions of peridotite, gabbro and pyroxenite occur within the metasediments. In the northern part of the area, these were very largely converted to bodies of ortho-amphibolite, which may show either gradational or local intrusive contacts with the surrounding rocks. Later metasomatic and hydrothermal activity converted many of these bodies wholly or partly to tremolite actinolite rocks and soapstone (Bloomfield & Garson, 1965).

The more important mineral occurrences include asbestos, gold, kyanite, limestone and phosphate, as well as large deposits of cerium-rich monazite, strontianite and manganese minerals (Bloomfield & Garson, 1965). The geologic map of the study area is depicted in Figure 2.

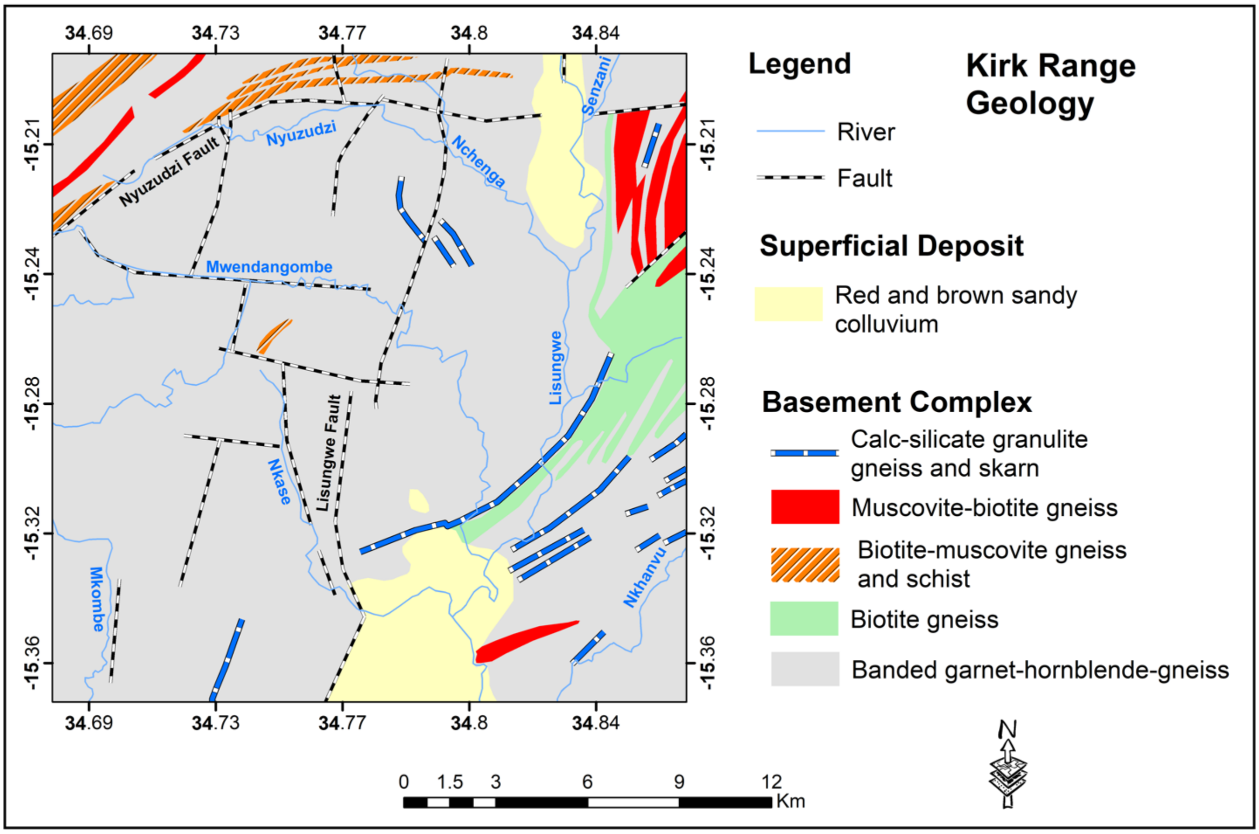

Figure 3: Study area geology

1.4 Data

Advanced Spaceborne Thermal Emission and Reflection Radiometer (ASTER) is an advanced multispectral satellite imaging system that was launched on board of the TERRA spacecraft in December 1999 by NASA and METI (Japan's Ministry of Economic Trade and Industry) (Li et al., 2011). The satellite measures reflected radiation in VNIR (0.52 and 0.86 μm), SWIR (1.6 to 2.43 μm), and emitted radiation in TIR wavelength region (8.125 to 11.65μm) with 3, 6, 5 bands and 15m, 30m, 90m resolution, respectively (Table 1). The swath-width is 60 km. The ASTER image used was ASTER L1T radiance data, which is calibrated at-sensor radiance, ortho-rectified, and precision terrain corrected; this data was acquired freely from the United States Geological Survey (USGS) Earth Explorer portal through their website (https://earthexplorer.usgs.gov/).

The ASTER data used in this study was acquired on 22 October 2004, in the summer to ensure less vegetation, low cloud cover, and high sun angle images were obtained.

Table 1: ASTER data specification

	ASTER	
Band	**Wavelength (µm)**	**Resolution (m)**
1 – Visible Green/Yellow	0.520-0.600	15
2 – Visible Red	0.630-0690	15
3 – NIR	0.760-0.860	15
4 – SWIR	1.600-1.700	30
5 – SWIR	2.145-2.185	30
6 – SWIR	2.185-2.225	30
7 – SWIR	2.235-2.285	30
8 – SWIR	2.295-2.365	30
9 – SWIR	2.360-2.430	30
10 – TIR	8.125 – 8.475	90
11 – TIR	8.475 – 8.825	90
12 – TIR	8.925 – 9.275	90
13 – TIR	10.250 – 10.950	90
14 – TIR	10.950 – 11.650	90

2. Methods

The ASTER Imagery was opted for in this study due to its combination of the channel subsystems design and moderate spectral resolution specifications. The Visible Near Infrared (VNIR) subsystem is used to obtain optical images with a spatial resolution of 15 m. The shortwave infrared (SWIR) subsystem also gets optical images with six band multiple bands, with a spatial resolution of 30m. The methodology adopted in this research is summarized in the methodology flow diagram (Figure 4). This research used the multispectral remote sensing data ASTER as the primary dataset and the geological and structural maps of the study area as secondary data. In this study, alteration mineral groups were detected using band ratios and spectral analysis using ENVI 5.3, and geological structures were automatically delineated using PCI Geomatica 2015.

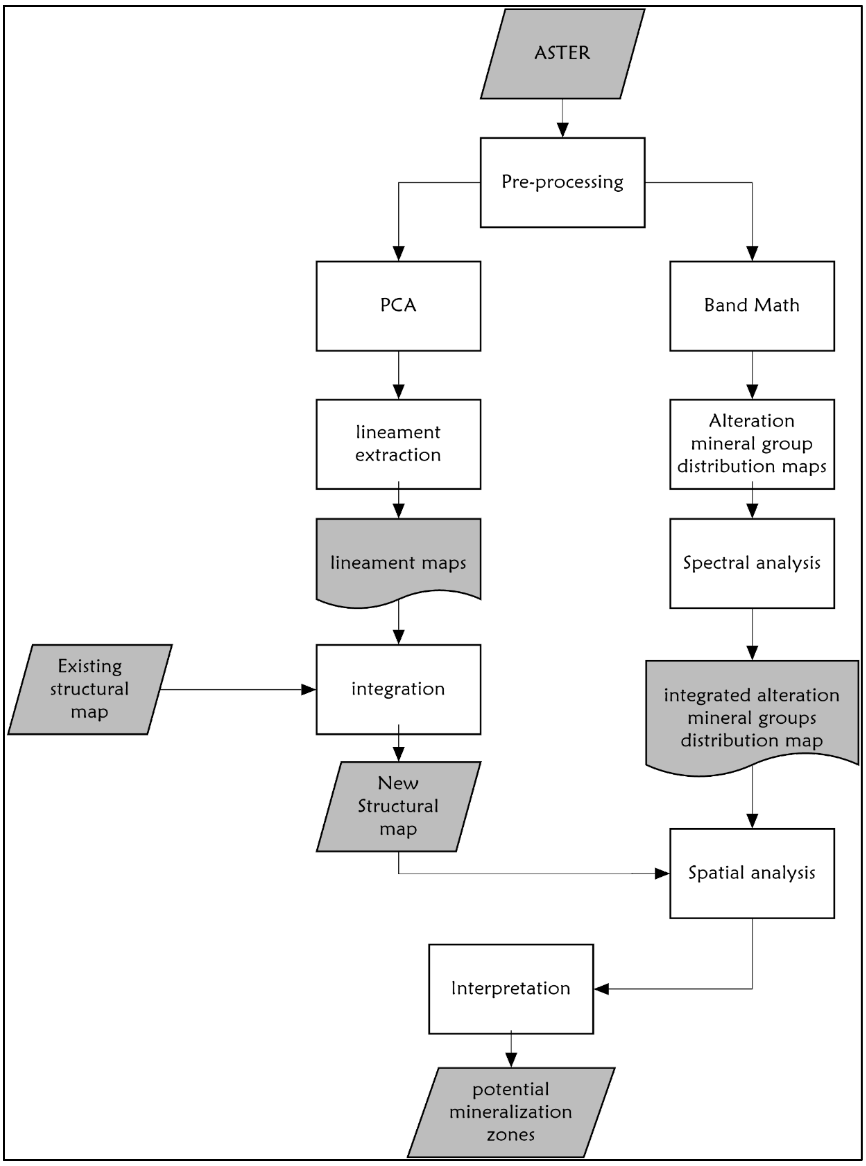

Figure 4: Methodology flow diagram

2.1 Data pre-processing

To take advantage and make good use of remote sensing data, we must be able to extract meaningful information from the imagery (Gupta, 2003). Several pre-processing techniques and steps were performed on the ASTER imagery before the various image processing techniques were applied. The ASTER L1T terrain precision radiance data was layer stacked and resampled to 15m VNIR spatial resolution using Nearest neighbor algorithm.

The layer stacked 9 bands of radiance ASTER VNIR-SWIR image was radiometrically and atmospherically corrected to an ASTER VNIR-SWIR reflectance image using the module fast line-of-sight atmospheric analysis of spectral hypercubes (FLAASH) in ENVI 5.3. FLAASH uses MODTRAN4 radiation transfer models for the calculations (Fatima et al., 2017; Ghulam, 2009). This method has shown to be better than others for mineral mapping (ENVI, 2009; Testa et al., 2018). Atmospheric parameters (i.e., total water vapour and CO_2 concentrations) for the date of the scene acquisition were obtained from the image header file. A tropical (T) atmospheric model and 80 km visibility were used as parameters in the model. After the atmospheric correction, the resulting unit of the new imagery was reflectance. A visual inspection of the spectral profiles for minerals showed considerable improvement after the atmospheric correction (Figure 5).

A Normalized Difference Vegetation Index (NDVI) was calculated from the ASTER reflectance image, and using a concurrent visual inspection of ASTER false colour composite RGB 321. The NDVI image and it's horizontal profile, were used to create a region of interest with band threshold value minimum 0.58, which covered green vegetation. This region of interest were used to build the vegetation mask. Using the same approach, cloud shadow and water masks were produced. Using a concurrent visual inspection of ASTER false colour composite RGB 321 and ASTER band 1 greyscale image and band 1 image horizontal profile, a region of interest was created from band threshold value minimum 0.19, which covered clouds and this region of interest was used to build the cloud mask. For cloud shadow and water mask, a concurrent visual inspection of ASTER false colour composite RGB 321 and ASTER band 2 greyscale image and band 2 image horizontal profile were used, thereafter a region of interest was created from band threshold value maximum 0.07, which covered cloud shadows and water; The last step involved building an integrated mask that was applied to the ASTER VNIR-SWIR reflectance image.

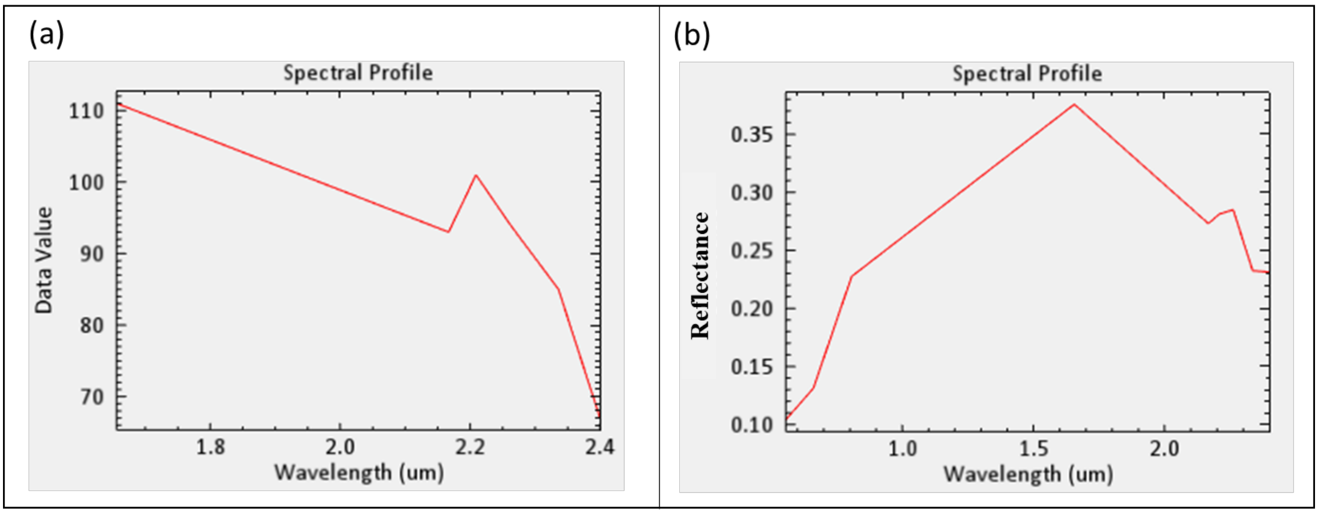

Figure 5: ASTER VNIR-SWIR (a) Z spectrum of radiance data before atmospheric correction, (b) Z spectrum for reflectance data after atmospheric correction.

2.2 Band Ratio

ASTER band ratios were performed to detect hydrothermal mineralization zones for further exploration. This approach includes all logical mathematical operations applied to individual digital numbers (DN) of bands (Gad & Kusky, 2007; He et al., 2010). Band ratio is a technique where the DN values of one band is divided by the DN value of another band. According to Cudahy (2011), band ratios are based on discrete characteristics of the absorption features of the minerals present in the area. As such, are useful in highlighting hydrothermal mineralization that cannot be seen in the raw bands (Inzana et al., 2003). This is a common approach in mapping hydrothermal alteration mineralization since it is not affected by illumination and topographical effects and at the same time suppresses reflectance albedo variations (Chinkaka, 2019).

This research adopted three band ratios developed by Cudahy (2011) to identify hydrothermal alteration mineral group content. Ferric oxide (FeO) content (hematite, goethite, jarosite) was identified using the band ratio B4/B3. A linear enhancement technique with stretch values lower limit of 1.1 and upper limit of 2.1 were applied. The blue shade indicates is low abundance, and red shade indicates high abundance. Aluminium hydroxide (Al-OH) content (phengite, muscovite, patagonite, illite, montmorillonite, kaolinite, dickite) was identified using the band ratio (B5+B7)/B6 with linear enhancement technique stretch value of 2.0 for lower limit and value of 2.25 for upper limit. The blue shade indiating low abundance, and red indicating high abundance. Magnesium hydroxide (Mg-OH) content (calcite, dolomite, magnesite, chlorite, epidote, talc, serpentine) was identified using the band ratio (B6+B9)/(B7+B8) with linear enhancement technique stretch values 1.05 and 1.2 for the lower and upper limits respectively.

Table 2: Hydrothermal alteration mineral group ASTER band ratio and enhancement parameters

Hydrothermal Alteration Mineral Group content	**Band ratio operation**	**Linear enhancement Stretch value**	
		Lower limit	Upper limit
FeO	B4/B3	1.1	2.1
Al-OH	(B5+B7)/B6	2.0	2.25
Mg-OH	(B6+B9)/(B7+B8)	1.05	1.2

2.3 Spectral Analysis

Spectral comparison of the images spectral reflectance curves was made using the mapped band ratio mineral contents by extracting the hydrothermal alteration mineral groups spectral signatures and comparing them with the USGS spectral signatures of the mineral group signatures in an attempt to assess the mineral spectra of the ASTER data. The USGS mineral spectral libraries were resampled to ASTER and various mineral spectra profiles from each alteration group were extracted and compared with ASTER image extracted spectral profiles of the hydrothermal alteration mineral groups (Mars & Rowan, 2011).

2.4 Principal Component Analysis

The Principal Component Analysis (PCA) was performed on ASTER multispectral image as an image enhancement technique in order to highlight the lineament structural information. PCA is a multivariate statistical technique that selects uncorrelated linear combinations (eigenvector loadings) of variables so that each component extracts linear combination and has a smaller variance. PCA is a well-known method for image enhancement to identify surface lineament structures (Li et al., 2011). It is more efficient in the identification of lineaments as compared to other image enhancement techniques such as histogram equalization, and high pass filters. (Shirmard et al., 2020). The result of this method was nine uncorrelated Principal Component (PC) bands. The first three PC bands can be used for structural mapping purposes, where PC band 1 contains most of the data variability, dominated by brightness differences caused by variation of surface topographic slope directions, with respect to the sun position, and often displays important structural information, PC band 2 contains the second most variability, and is orthogonal to PC band 1 in (ɳ) directional space and PC band 3 contains the third most variability and is orthogonal to the other two PC bands (Ali & Pour, 2014; Cadavid et al., 2008). PC band 1 from the ASTER image was selected for mapping lineaments.

2.5 Geological Lineament Extraction

Geological lineament were automatically extracted from an enhanced ASTER PC 1 band using a LINE module algorithm in PCI Geomatica software. The LINE module algorithm accepts the input of an 8-bit grey scale image (Ibraheem et al., 2019; Sukumar & Nelson, 2017). Knowledge of existing known lineaments from published geological and structural map of the study area by Bloomfield & Garson (1965) was used as reference for the extraction process. According to Hashim et al, (2013), the LINE module delineates lineaments in three main stages. These steps include Edge detection, Thresholding, and Curve extraction as illustrated in Figure 6.

Figure 6: Execution flowchart for the LINE Module algorithm automatic lineaments extraction

The steps were executed over The ASTER PC 1 images with six optimal parameters as model calibrators for the LINE module algorithm to control the automatic process of lineament extraction as shown in Table 3.

Table 3: Optimal parameter values used to map lineaments of ASTER PC band 1 of the study area.

PARAMETER	VALUE
Filter Radius	15
Threshold For Edge Gradient	100
Threshold For Curve Length	38
Threshold For Line Fitting Error	1
Threshold For Angular Difference	15
Threshold For Linking Distance	80

2.6 Geological Lineaments kinematics and orientation

The lineaments kinematics and orientation were derived from the new structural dataset mainly based on the kinematic indicator of displaced lineament features using Rose Diagram software version 2017. The orientation angles from the Rose diagram were used to identify the tectonic mobile belts that have contributed to the structural mineratization of the area.

2.7 Spatial Analysis

The mapped surface structures from PCA transform images were visually compared to existing geological structures of the study area and then integrated. Surface structures reflect subsurface structures this helped in the assessment of ASTER imagery in the mapping of surface features (Li et al., 2011). This was done to help develop the final geological surface structures from which observational spatial analysis was done with alteration zones to locate the potential mineralization areas within the area.

3. Results

3.1 ASTER Band Ratio

Ferric oxide (FeO) content (hematite, goethite, jarosite) was identified using the band ratio B4/B3 with linear enhancement technique having the following stretch values lower limit 1.1 and upper limit 2.1. Aluminium hydroxide (Al-OH) content (phengite, muscovite, patagonite, illite, montmorillonite, kaolinite, dickite) was identified using the band ratio (B5+B7)/B6 with linear enhancement technique having the following stretch values lower limit 2.0 and upper limit 2.25.

Magnesium hydroxide (Mg-OH) content (calcite, dolomite, magnesite, chlorite, epidote, talc, serpentine) was identified using the band ratio (B6+B9)/(B7+B8) with linear enhancement technique having the following stretch values lower limit 1.05 and upper limit 1.2 where blue is low abundance and red is high abundance. The band ratio results are shown in Figure 7.

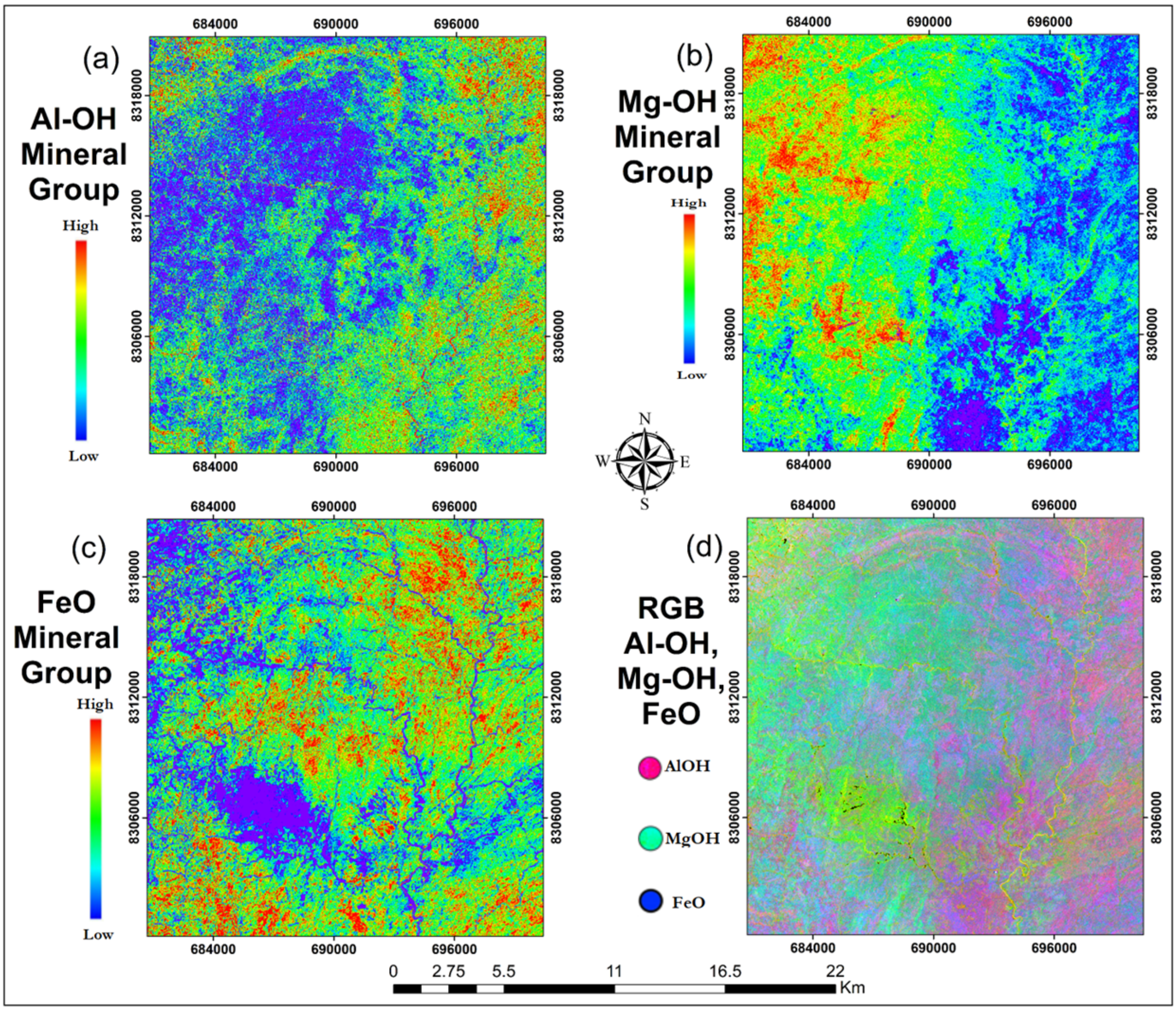

Figure 7: ASTER band ratio operations results showing hydrothermal alteration mineral groups. (a) FeO mineral group, (b) Al-OH mineral group, (c) Mg-OH mineral group and (d) false colour composite image R=(Al-OH): G=(Mg-OH): B=(FeO).

3.2 ASTER Spectral Analysis

Using the ASTER band ratio images of the hydrothermal alteration minerals spectral profiles of each were extracted for the high content areas and then compared to USGS ASTER resampled spectral profiles of different minerals in each group. This was done to validate the mapped hydrothermal alteration mineral groups (Waldhoff et al., 2008). The spectral profiles showed similarities but not perfectly similar due to the mixture of various mineral types within a group which ASTER cannot accurately segregate (Figure 8).

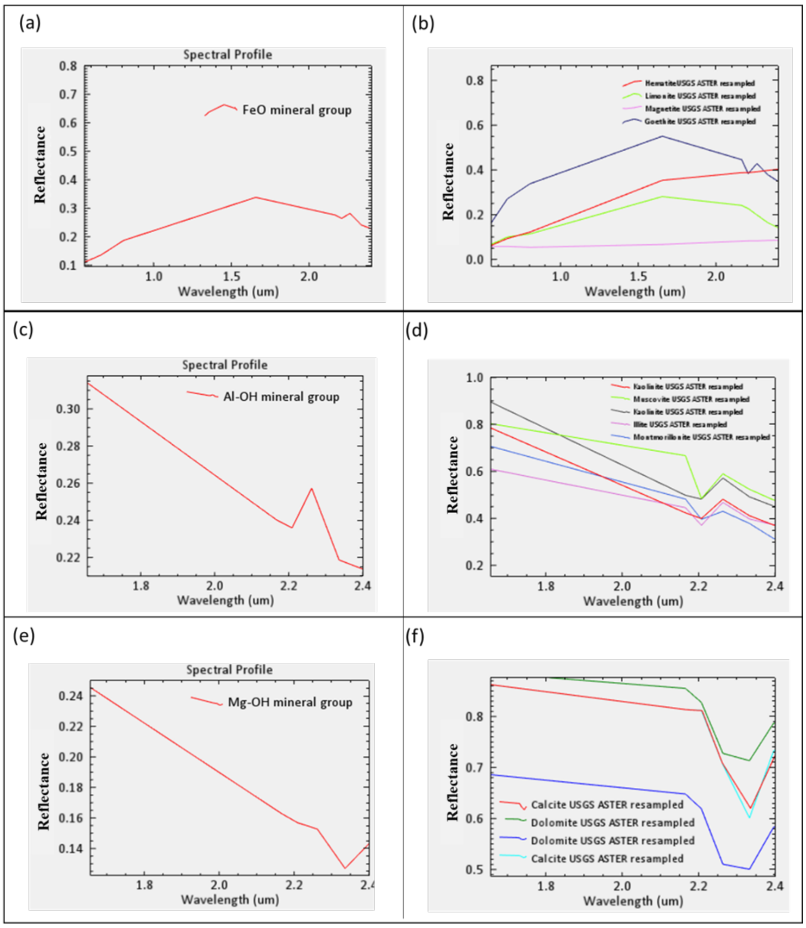

Figure 8: Spectral profiles a, c and e represent ASTER extracted spectral profiles for FeO, Al-OH and Mg-OH contents respectively and Spectral profiles b, d and f represent USGS ASTER resampled spectral profiles of minerals in each mineral group.

3.3 ASTER Geological Lineament Extraction

The automatically extracted lineaments from ASTER PC band 1 results are presented in Figure 9. The lineaments show a dominant direction in the NE – SW direction and a minor one in the W – E direction.

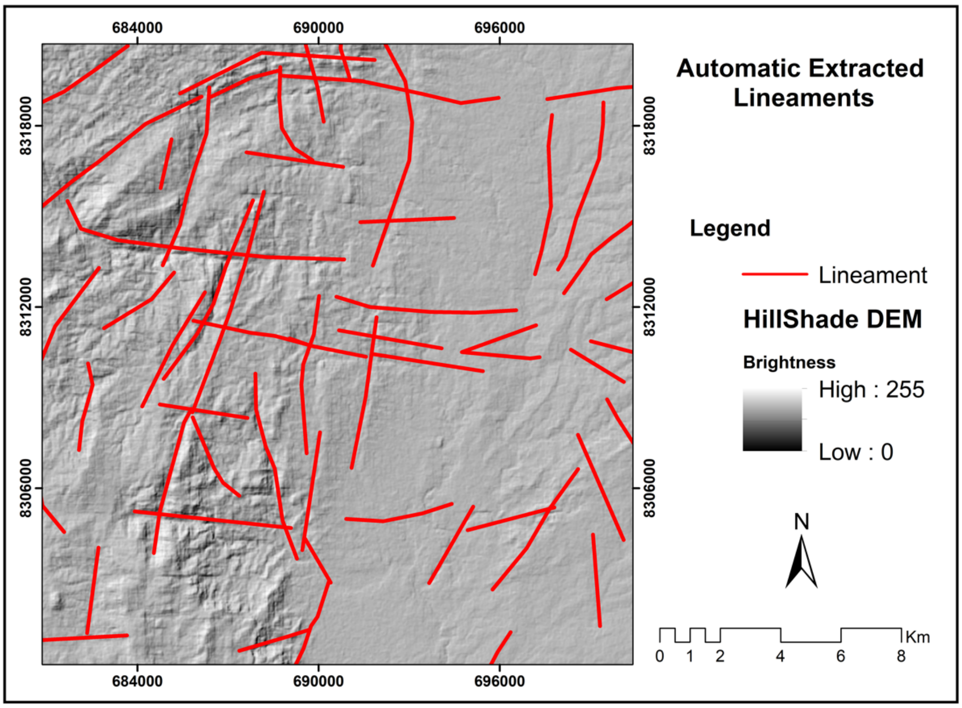

Figure 9: ASTER extracted lineaments draped on a hillshaded Digital Elevation Model (DEM)**.**

3.4 Integrated ASTER extracted Lineaments and published structural map of the study area

The extracted ASTER lineaments map was visually compared to the existing structural map of the study area. This operation was done to show the improvements and differences between the two lineament maps. The final updated lineaments map was then produced, thus combining the lineaments from the ASTER image and existing published geological map of the area. The published existing map of the area by Geological Survey Department of Malawi shows most of the lineament structures. Several new structures were observed in the updated lineament structural map, as shown in Figure 10.

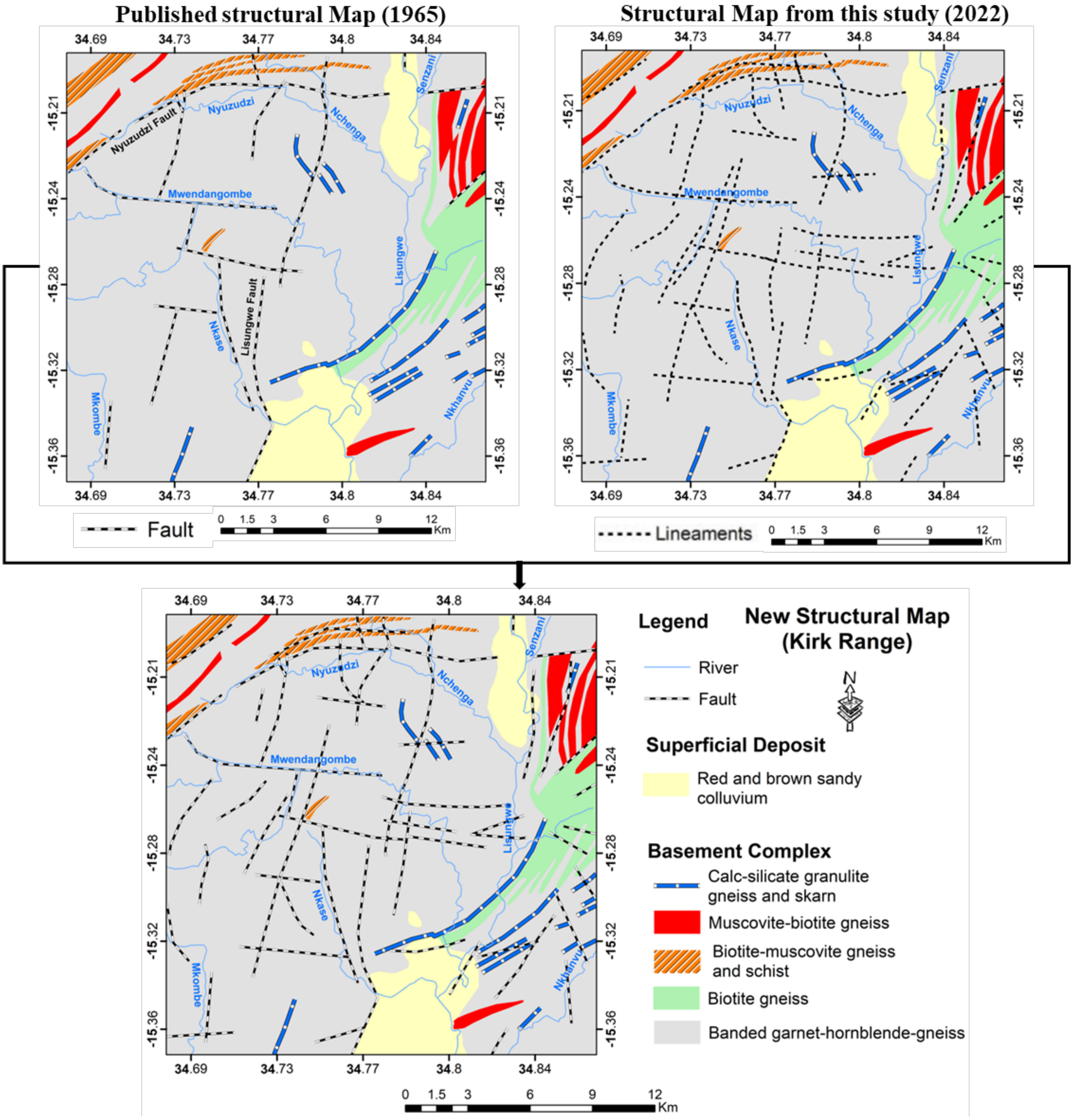

Figure 10: Combination of ASTER extracted lineaments and published Lineaments to produce a New Geological Structural Map for the Kirk range – Lisungwe area.

3.5 Geological Lineament analysis and tectonic interpretation

The study area has two trending geological lineament patterns NE-SW and E-W directions (Figure 11a). Orientation analysis shows that the NE-SW dominant orientation angle is at 15 degrees and the minor E-W direction at about 90 degrees. Further analysis results of the kinematics and sense of motion as shown in Figure 11(b) indicate that the two sharp orientations of the lineament structures in the study area represent two distinct Precambrian tectonic episodes that have affected the study area: The Ubendian and Irumedi Orogeny. These orogenies were then overprinted by the Pan African Mozambician Mobile episode (Ring & Betzler, 1993) . Figure 11(b) indicates lineament kinematics of the maximum principal force $\sigma 1$, (shear fracture) in the NE-SW direction and the minimum principal force $\sigma 3$ at a perpendicular angle to the maximum principal force moving in the E-W direction. Therefore, these two tectonic forces influence hydrothermal alteration mineralization in the study area.

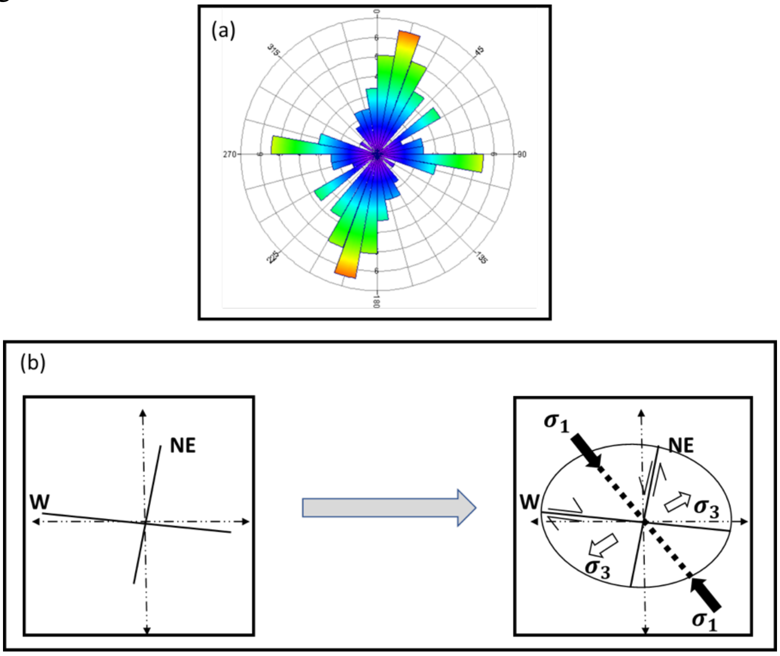

Figure 11: Rose diagram orientation of geological lineamnets showing dominant NE – SW and a minor W – E direction (a) and geological lineaments kinematics diagram indicating tectonic episodes in the Kirk range – Lisungwe area

3.6 Observation Spatial Analysis

The newly mapped structural lineaments were overlayed on the hydrothermal alteration mineral map (Figure 12). Based on this, the results indicate that the alteration mineralization correlate with the spatial location of the geological lineament structures.

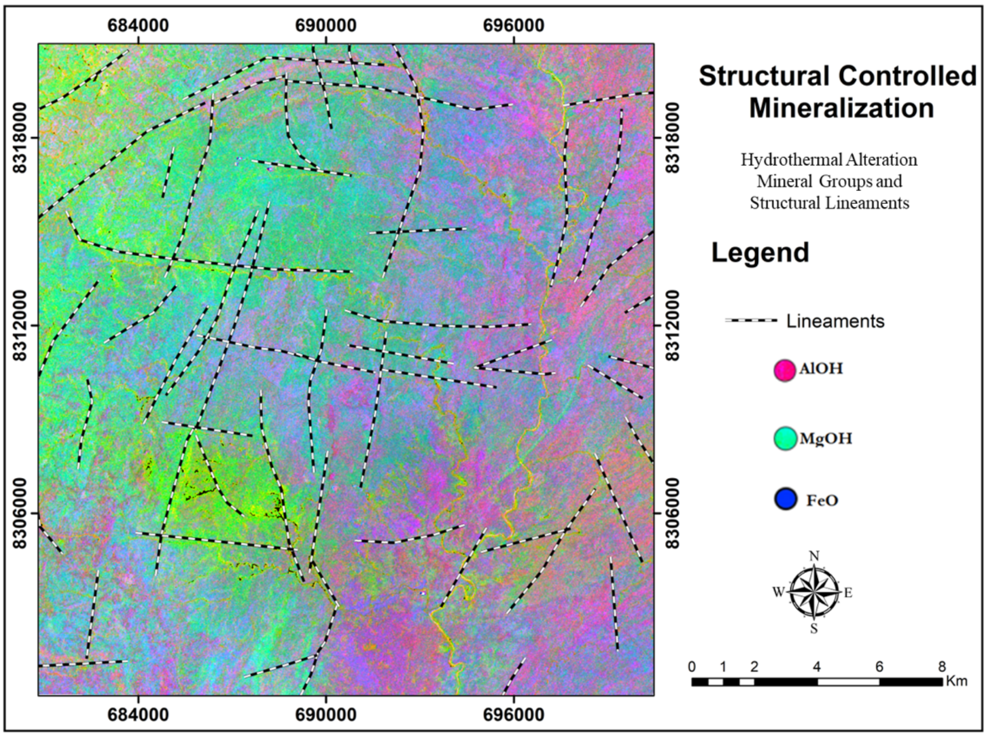

Figure 12: RGB: Al-OH, Mg-OH and FeO Hydrothermal Alteration Mineral Groups structurally controlled.

4. Discussion

4.1 Hydrothermal alteration mineral groups and Spectral analysis

ASTER band ratio results shown in Figure 7 were based on the absorption features of the specific alteration groups. The band ratio result images show the areas with intense alteration of the mineral groups of concern. This means that in the mineral content map, the red colour indicates high presence and concentrartion of the alteration minerals in the specific group. The FeO which contain minerals such as hematite and goethite, is the main mineral group content present in the area ranging from moderate to high values on the scale bar as shown in Figure 7(c), seconded by Mg-OH/Carbonate indicated in Figure 7(b), and then Al-OH content is the least in the area (Figure 7a). The Al-OH are more concentrated in the left top corner of the area and on the right side along the Lisungwi river. The Al-OH content of clay minerals like muscovite, illite, montmorillonite, kaolinite and dickite. Figure 7(b) depicts high presence and concentration of Mg-OH content on the left side of the study area. These hydrothermal minerals include calcite and dolomite. These minerals are more common in the Phalula, Zalewa and Senzani area and were also mapped by Bloomfield & Garson (1965) using conversational and traditional mapping methods. As seen in the band ratios (Figure 7), the delineated lineaments are clearly seen as linear features and confirm the lineaments analysis in sections 3.5 and 3.6. The mapped linear structures orientation directions are visually captured in the individual band ratios in the NE-SW and E-W directions. This means that the hydrothermal mineralization style follows the structural patterns of lineaments. The new structural lineaments shown in Figure 10 coincide mostly with the mineral group contents, particularly Al-OH and Mg-OH/ Carbonate in the northeast, western parts and the north curved lineaments of the in the study area which correspond with the mapped new structures. The combined Red/Green/Blue of Al- OH/Mg-OH/FeO respectively in Figure 12 shows the spatial and structural relationships of the mineralization with the new lineament structures.

4.2 Geological Lineaments from ASTER image and their directions

Geological linemaments are significant in solving the problems raised during pre-exploration activities. Crowded micro lineaments alone with the macro lines are the best place for minerals exploration. (Sukumar & Nelson, 2017). Commonly, tectonic lineaments are extracted using edge enhancement and segmentation techniques; hence this research employed the LINE module algorithm, which proved to be useful as it detected geological lineaments in correlation to existing faults in the study area. As shown in Figure 11(b), the Kirk range - Lisungwe area is characterized by two main structural lineament patterns in the NE-SW and W-E directions. It means that NE-SW lineament structures were formed due to the tectonic force direction in the NW-SE direction perpendicular to the lineament directions and the W-E lineament structures were formed due to the tectonic force direction in the N-S direction. Figure 11(b) shows that these tectonic forces resulted in strike-slip extensional faulting. These geological structures are potential conduits for fluid flow resulting in hydrothermal mineralization. The study further observed that the hydrothermal alteration zones are structurally controlled. Structural lineaments and hydrothermal alteration minerals are used to identify potential mineralization zone as the combination of the two shows that alteration are due to the hydrothermal fluids emanating from within, which can lead to mineralization (Manuel et al., 2017). The assessment of alteration and lineament map of this area showed that areas of alteration to the west of the study area show distinctive structural control where Mg-OH alterations are dominant. These areas have been identified in this study as high potential mineralized areas and worth further exploration investigation (Figure 13). Therefore, mineral exploration in the Kirk range should be done along the geological lineament structures.

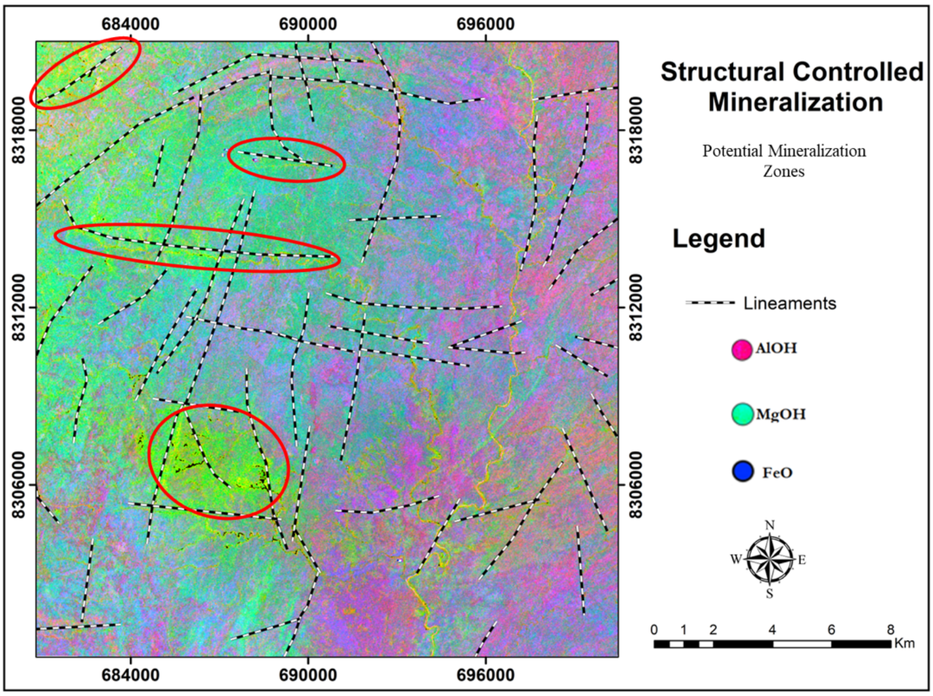

Figure 13: Potential exploration sites (red circles) with structural controlled mineralization

5. Conclusion

This research presented the potential zones of hydrothermal mineralization within the Kirk range – Lisungwe area and further generated an updated geological lineament structural map. This has been accomplished through various processing techniques using ASTER L1T imagery data. ASTER band ratio operations successfully mapped various alteration mineral zones, including FeO minerals (hematite, goethite), Al-OH clay minerals (muscovite, illite, montmorillonite, kaolinite, dickite) and Mg-OH minerals (calcite, dolomite, magnesite, chlorite, epidote, talc, serpentine). This shows that the Kirk range – Lisungwe area has hydrothermal alteration potential that could probably be associated with high economic value minerals like copper, silver and gold. This led to the successful application of band ratio indices for mineral exploration activities. Spectral analysis validated the detected spectral mineral groups using the USGS laboratory ASTER resampled mineral spectral profiles. Automatic extraction algorithm was applied to map the surface expression of geological structures (lineaments), which was accomplished on ASTER PC 1 enhanced image. The study revealed that the hydrothermal mineralization in the study area is structurally controlled. This is evident from the new structural map that this study has developed. This means that further exploration targets for mineral exploration companies in the area should focus on shear zones and geological lineaments and that remote sensing techniques that were explored in this study may be applied in remote and inaccessible areas to help delineate potential mineral deposits at the surface.

6. Acknowledgments

The authors would like to thank the Malawi University of Science and Technology, Department of Geological Surveys of Malawi for providing the geological map and United States Geological Survey for the freely available ASTER satellite data used in this study.

7. Author Contributions

Emmanuel Chinkaka: Conceptualization, Formal analysis, Cartographic Map Design, Writing, Review **Francis Kapakasa**: Data Pre-processing, Data analysis, Writing, **Chikondi Chisenga:** Reviewing, Editing, **Richard Mvula:** Reviewing, Editing, **Wilson Tchongwe:** Reviewing, Editing, **Kyle F. Davis**: Augmentation, Review.

8. Funding

This research did not receive any funding.

9. Declaration of conflict of interest

The authors declare that they have no known competing financial interests or personal relationships that could have appeared to influence the work reported in this paper.

10. References

Ali, A., & Pour, A. (2014). Lithological mapping and hydrothermal alteration using Landsat 8 data: a case study in ariab mining district, red sea hills, Sudan. *International Journal of Basic and Applied Sciences*, *3*(3). https://doi.org/10.14419/ijbas.v3i3.2821

Bloomfield, K., & Garson, M. S. (1965). *The Geology of the Kirk Range -Lisungwe valley area*.

Cadavid, A. C., Lawrence, J. K., & Ruzmaikin, A. (2008). Principal components and independent component analysis of solar and space data. *Solar Physics*, *248*(2), 247–261. https://doi.org/10.1007/s11207-007-9026-2

Chinkaka, E. (2019). Integrating Worldview-3, ASTER and Aeromagnetic Data for Lineament Structural Interpretation and Tectonic Evolution of the Haib Area, Namibia (MSc Thesis). University of Twente, Faculty ITC, February, 81.

Chisambi, J., & von der Heyden, B. (2019). Primary gold mineralization in the lisungwe valley area, kirk range, southern Malawi. *South African Journal of Geology*, *122*(4), 505–518. https://doi.org/10.25131/sajg.122.0039

Chiwona, A. G., Cortés, J. A., Gaulton, R. G., & Manning, D. A. C. (2020). Petrology and geochemistry of selected nepheline syenites from Malawi and their potential as alternative potash sources. *Journal of African Earth Sciences*, *164*(July 2019), 103769. https://doi.org/10.1016/j.jafrearsci.2020.103769

Cudahy, T. (2011). *Satellite ASTER Geoscience Product Notes for Western Australia*. *2*(Version 1), 1–26.

ENVI. (2009). ENVI Atmospheric Correction Module: QUAC and FLAASH user's guide. *Module Version*, 44. http://scholar.google.com/scholar?hl=en&btnG=Search&q=intitle:ENVI+Atmospheric+Correction+Module:+QUAC+and+FLAASH+user's+guide#0

Fatima, K., Khan Khattak, M. U., Kausar, A. B., Toqeer, M., Haider, N., & Rehman, A. U. (2017). Minerals identification and mapping using ASTER satellite image. *Journal of Applied Remote Sensing*, *11*(04), 1. https://doi.org/10.1117/1.jrs.11.046006

Gad, S., & Kusky, T. (2007). ASTER spectral ratioing for lithological mapping in the Arabian-Nubian shield, the Neoproterozoic Wadi Kid area, Sinai, Egypt. *Gondwana Research*, *11*(3), 326–335. https://doi.org/10.1016/j.gr.2006.02.010

Ghulam, A. (2009). How to calculate reflectance and temperature using ASTER data. *Saint Louis University GIS Portal*, 1–6.

Gupta, R. P. (2003). *Remote Sensing Geology.*

Haroni, H., & Lavafan, A. (2007). Integrated Analysis of ASTER and Landsat ETM Data to Map Exploration Targets in the Muteh Gold-Mining Area, IRAN. *5th International Symposium on Spatial Data Quality, …*. http://www.itc.nl/ISSDQ2007/proceedings/P ostersession/ASADI.pdf

He, Z., He, B., & Ying, C. (2010). Hydrothermal alteration mapping using ASTER data in East Kunlun Mountains, China. *International Geoscience and Remote Sensing Symposium (IGARSS)*, 4514–4517. https://doi.org/10.1109/IGARSS.2010.5651085

Ibraheem, I. M., Haggag, M., & Tezkan, B. (2019). Edge detectors as structural imaging tools using aeromagnetic data: A case study of Sohag area, Egypt. *Geosciences (Switzerland)*, *9*(5). https://doi.org/10.3390/geosciences9050211

Inzana, J., Kusky, T., Higgs, G., & Tucker, R. (2003). Supervised classifications of Landsat TM band ratio images and Landsat TM band ratio image with radar for geological interpretations of central Madagascar. *Journal of African Earth Sciences*, *37*(1–2), 59–72. https://doi.org/10.1016/S0899-5362(03)00071-X

Li, N., Frei, M., & Altermann, W. (2011). Textural and knowledge-based lithological classification of remote sensing data in Southwestern Prieska sub-basin, Transvaal Supergroup, South Africa. In *Journal of African Earth Sciences* (Vol. 60, Issue 4). https://doi.org/10.1016/j.jafrearsci.2011.03.002

Manuel, R., Brito, M. da G., Chichorro, M., & Rosa, C. (2017). Remote sensing for mineral exploration in central Portugal. *Minerals*, *7*(10). https://doi.org/10.3390/min7100184

Mars, J. C., & Rowan, L. C. (2011). ASTER spectral analysis and lithologic mapping of the Khanneshin carbonatite volcano, Afghanistan. *Geosphere*, *7*(1), 276–289. https://doi.org/10.1130/GES00630.1

Ring, U., & Betzler, C. (1993). Architecture, Tectonics and Sedimentology of the Malawi Rift (East Africa). *Zeitschrift Der Deutschen Geologischen Gesellschaft*, *144*(1), 30–44. https://doi.org/10.1127/zdgg/144/1993/30

Shirmard, H., Farahbakhsh, E., Beiranvand Pour, A., Muslim, A. M., Müller, R. D., & Chandra, R. (2020). Integration of Selective Dimensionality Reduction Techniques for Mineral Exploration Using ASTER Satellite Data. *Remote Sensing*, *12*(8), 1261. https://doi.org/10.3390/rs12081261

Sukumar, M., & Nelson, C. (2017). Performance evaluation of lineament extraction methods in ASTER satellite images. *International Journal of Oceans and Oceanography*, *11*(2), 249–263. http://www.ripublication.com

Testa, F., Villanueva, C., Cooke, D., & Zhang, L. (2018). Lithological and Hydrothermal Alteration Mapping of Epithermal, Porphyry and Tourmaline Breccia Districts in the Argentine Andes Using ASTER Imagery. *Remote Sensing*, *10*(2), 203. https://doi.org/10.3390/rs10020203

Waldhoff, G., Bubenzer, O., Bolten, A., Koppe, W., & Bareth, G. (2008). Spectral analysis of aster, hyperion, and Quickbird data for geomorphological and geological research in Egypt (Dakhla Oasis, western desert). *International Archives of the Photogrammetry, Remote Sensing and Spatial Information Sciences - ISPRS Archives*, *37*, 1201–1206.

Yong-gui, Z., Zheng-le, C., Xing-tong, C., & Bai-lin, C. (2014). Alteration zone mapping for detecting potential mineralized areas in Kaladawan of north altyn tagh using ASTER data. *IOP Conference Series: Earth and Environmental Science*, *17*, 012173. https://doi.org/10.1088/1755-1315/17/1/012173

Zhang, T., Yi, G., Li, H., Wang, Z., Tang, J., Zhong, K., Li, Y., Wang, Q., & Bie, X. (2016). Integrating Data of ASTER and Landsat-8 OLI (AO) for Hydrothermal Alteration Mineral Mapping in Duolong Porphyry Cu-Au Deposit, Tibetan Plateau, China. *Remote Sensing*, *8*(11), 890. https://doi.org/10.3390/rs8110890

Zhou, Y. G., Chen, Z. Le, Chen, X. T., & Chen, B. L. (2014). Alteration zone mapping for detecting potential mineralized areas in Kaladawan of north altyn tagh using ASTER data. *IOP Conference Series: Earth and Environmental Science*, *17*(1). https://doi.org/10.1088/1755-1315/17/1/012173